Synthesis and Reactions of Novel Triply Thiolate-Bridged Diiron Complexes [Cp*Fe(μ_2-SR)$_3$FeCp*] (Cp* = η^5-C$_5$Me$_5$; R = Et, Ph)

Yanhui Chen, Yuhan Zhou, and Jingping Qu*

State Key Laboratory of Fine Chemicals, School of Chemical Engineering, Dalian University of Technology, Dalian 116012, People's Republic of China

Received December 8, 2006

The novel thiolate-bridged diiron complexes [Cp*Fe(μ_2-SR)$_3$FeCp*] (**1**, R = Et; **2**, R = Ph) have been obtained by the reaction of [Cp*FeCl]$_2$ with LiSEt or LiSPh in THF. Treatment of **1** with CO or CN^{t}Bu in THF gives complex [Cp*FeSEt(μ_2-SEt)$_2$FeCp*CO] (**3**) or [Cp*FeSEt(μ_2-SEt)$_2$FeCp*CN^{t}Bu] (**4**), while reaction of **1** with CN^{t}Bu in CH_2Cl_2 results in the formation of complex [Cl$_2$Fe(μ_2-SEt)$_2$FeCp*CN^{t}Bu] (**5**). These five complexes have been spectroscopically and crystallographically characterized. In addition, the formation of **5** indicates that this class of clusters might serve as carbon−halogen bond activation reagents (catalysts), and carbon−halogen bond cleavage reaction of **4** is also described.

Introduction

Iron−sulfur complexes have received increasing attention, owing to their unusual structures and occurrence in biological metalloproteins including nirtrogenase, hydrogenase, and ferredoxins.[1] Acting as the active sites in numerous proteins in various organisms, they usually serve as electron-transport functionalities and complete biological reactions through cooperative actions of many metal centers in the form of clusters.[2] So far, a large number of iron−sulfur (or thiolate) clusters with various structures have been synthesized and structurally determined, especially Fe_2S_2 complexes.[3] However, among synthetic thiolate-bridged diiron complexes, considerable efforts have been devoted to the studies on butterfly Fe_2S_2 clusters with carbonyl ligands, due mainly to their close relevance to hydrogenase,[4] and the analogous thiolate-bridged diiron cluster with single pentamethycyclopentadienyl (Cp*) ligands is less developed,[5] although the introduction of Cp* groups into the cluster can increase the electron density at the metal centers and cause the cluster to be more reactive. Recently, a series of diruthenium complexes with two or three bridging thiolate ligands such as [Cp*Ru(μ_2-SPr^i)$_2$RuCp*],[6] [Cp*Ru(μ_2-SPr^i)$_3$RuCp*],[7] and [Cp*RuCl(μ_2-SR)$_2$RuClCp*] (R = Me, Et, Pr^i, etc.)[8] have been reported. These complexes can provide well-defined bimetallic reaction sites for unique activation and transformation of organic substrates including alkynes, hydrazines, alkyl halides, and other transition metal compounds.[9] Situated in the same column, the iron counterparts of these ruthenium thiolate clusters are expected to have analogous properties of ruthenium clusters. However, so far, there has been no example of a diiron thiolate cluster with a Cp* as ancillary ligand. Here we report our preliminary results on the synthesis of diiron thiolate clusters with a single Cp* ligand on each Fe center, which provide bimetallic reaction sites and simulate biological metalloproteins to activate small molecules. The method of successful preparation of diiron thiolate complexes [Cp*Fe(μ_2-SR)$_3$FeCp*] (R = Et, Ph) together with their structures, brief reaction patterns with CO and CN^{t}Bu, and some of the chemistry dealing with carbon−halogen cleavage are described.

Results and Discussion

Synthesis and Characterization of [Cp*Fe(μ_2-SR)$_3$FeCp*] (1, R = Et; 2, R = Ph). As outlined in Scheme 1, treatment of [Cp*FeCl]$_2$[10] with 2 equiv of LiSEt in THF at −78 °C to

* To whom correspondence should be addressed. Fax: +86-411-8363-3080. E-mail: qujp@chem.dlut.edu.cn.

(1) (a) Coucouvanis, D. *Acc. Chem. Res.* **1991**, *24*, 1–8. (b) Darensbourg, M. Y.; Lyon, E. J.; Smee, J. J. *Coord. Chem. Rev.* **2000**, *206–207*, 533–561. (c) Karlin, K. D. *Science* **1993**, *261*, 701–708. (d) Rao, P. V.; Holm, R. H. *Chem. Rev.* **2004**, *104*, 527–559. (e) Song, L.-C. *Acc. Chem. Res.* **2005**, *38*, 21–28. (f) Koutmos, M.; Coucouvanis, D. *Angew. Chem., Int. Ed.* **2005**, *44*, 1971–1974. (g) Ott, S.; Kritikos, M.; Åkermark, B.; Sun, L.; Lomoth, R. *Angew. Chem., Int. Ed.* **2004**, *43*, 1006–1009.

(2) Noodleman, L.; Norman, J. G., Jr.; Osborne, J. H.; Aizman, A.; Case, D. A. *J. Am. Chem. Soc.* **1985**, *107*, 3418–3826.

(3) Ogino, H.; Inomata, S.; Tobita, H. *Chem. Rev.* **1998**, *98*, 2093–2121.

(4) (a) Song, L.-C.; Cheng, J.; Hu, Q.-M.; Gong, F.-H.; Bian, H.-Z.; Wang, L.-X. *Organometallics* **2005**, *24*, 472–474. (b) Song, L.-C.; Cheng, H.-W.; Hu, Q.-M. *Organometallics* **2004**, *23*, 1072–1080. (c) Song, L.-C.; Cheng, J.; Yan, J.; Wang, H.-T.; Liu, X.-F.; Hu, Q.-M. *Organometallics* **2006**, *25*, 1544–1547.

(5) (a) Madec, P.; Muir, K. W.; Pétillon, F. Y.; Rumin, R.; Scaon, Y.; Schollhammer, P.; Talarmin, J. *J. Chem. Soc., Dalton Trans.* **1999**, 2371–2383. (b) Wachter, J. *Angew. Chem., Int. Ed.* **1989**, 1613–1626.

(6) Takahashi, A.; Mizobe, Y.; Matsuzaka, H.; Dev, S.; Hidai, M. *J. Organomet. Chem.* **1993**, *456*, 243–253.

(7) Dev, S.; Mizobe, Y.; Hidai, M. *Inorg. Chem.* **1990**, *29*, 4797–4801.

(8) (a) Hidai, M.; Mizobe, Y.; Matsuzaka, H. *J. Organomet. Chem.* **1994**, *473*, 1–14. (b) Matsuzaka, H.; Qu, J.-P.; Ogino, T.; Nishio, M.; Nishibayashi, Y.; Ishii, Y.; Uemura, S.; Hidai, M. *J. Chem. Soc., Dalton Trans.* **1996**, 4307–4312.

(9) (a) Nishio, M.; Matsuzaka, H.; Mizobe, Y.; Tanase, T.; Hidai, M. *Organometallics* **1994**, *13*, 4214–4226. (b) Kuwata, S.; Mizobe, Y.; Hidai, M. *Inorg. Chem.* **1994**, *33*, 3619–3620. (c) Shimada, H.; Qu, J.-P.; Matsuzaka, H.; Ishii, Y.; Hidai, M. *Chem. Lett.* **1995**, 671–672. (d) Matsuzaka, H.; Takagi, Y.; Ishii, Y.; Nishio, M.; Hidai, M. *Organometallics* **1995**, *14*, 2153–2155. (e) Qu, J.-P.; Matsuzaka, H.; Ishii, Y.; Hidai, M. *Chem. Lett.* **1996**, 767–768. (f) Qu, J.-P.; Masui, D.; Ishii, Y.; Hidai, M. *Chem. Lett.* **1998**, 1003–1004.

(10) (a) Stephan, M.; Muller, P.; Zenneck, U.; Pritzkow, H.; Siebert, W.; Grimes, R. N. *Inorg. Chem.* **1995**, *34*, 2058–2067. (b) Shintani, R.; Fu, G. C. *Org. Lett.* **2002**, *4*, 3699–3702. (c) Takemoto, S.; Ogura, S.; Yo, H.; Hosokoshi, Y.; Kamikawa, K.; Matsuzaka, H. *Inorg. Chem.* **2006**, *45*, 4871–4873.

10.1021/om0611148 CCC: $40.75
Publication on Web 01/25/2008

Scheme 1

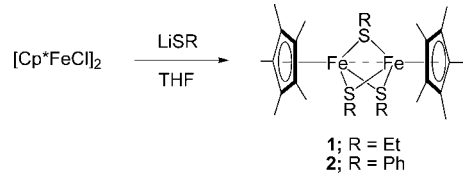

ambient temperature produces the complex [Cp*Fe(μ_2-SEt)$_3$FeCp*] (**1**) in 49% yield (based on $FeCl_2$) as a violet microcrystalline solid together with Cp*$_2$Fe (9% yield) and Fe(0) (15% yield). The formation of the mixed-valence **1** is rather unexpected compared with the formation of the Ru(II) dimer [Cp*Ru(μ_2-SPr^i)]$_2$ from [Cp*RuCl]$_4$ and NaSPr^i [6] and is very different from that of [Cp*Ru(μ_2-SEt)$_3$RuCp*] by the reaction of [Cp*RuCl$_2$]$_2$ and NaSEt, in which a part of NaSEt is consumed for the reduction of a Ru(III)−Ru(III) pair to a formal Ru(III)−Ru(II) pair.[7] Although the mechanism of the partial oxidation of the Fe center in the synthesis of **1** is currently unknown, in view of the byproduct of Cp*$_2$Fe and Fe(0), a redox reaction between the intermediate [Cp*Fe(μ_2-SEt)]$_2$ species and the residual [Cp*FeCl]$_2$ might be a possibility. Such an analogous redox phenomenon has also been observed in the synthesis of [(Cp*Fe)$_2$(μ_2-NHPh)(μ_2-NPh)] from [Cp*FeCl]$_x$ and LiNHPh.[10] Complex **1** is paramagnetic at room temperature; the EPR spectrum of a powder sample exhibits a rhombic signal at $g = 2.00$. The ^{1}H NMR spectrum of **1** in C_6D_6 shows three broad signals at δ −20.06, −4.23, and 46.77 ppm attributed to two equivalent Cp* protons, three equivalent CH_3 protons, and three equivalent CH_2 protons, respectively. A similar reaction of LiSPh affords the complex [Cp*Fe(μ_2-SPh)$_3$FeCp*] (**2**) in 55% yield as blue microcrystals. The ^{1}H NMR spectrum of **2** exhibits a resonance for Cp* protons at δ −23.87 ppm, which significantly shifts upfield compared with that observed for **1**, and three sets of resonances due to the benzene groups. Both **1** and **2** are unambiguously characterized by single-crystal X-ray diffraction analysis, and their spectral features are fully consistent with their crystal structures. The crystallographlic data as well as bond distances and angles are presented in Tables 1 and 2.

An ORTEP drawing of **1** is shown in Figure 1. Two Cp* ligands coordinate to the Fe centers with their C_5 planes perpendicular to the Fe−Fe vector, and the dihedral angle between the Cp* rings is only 4.3°. The three thiolate ligands coordinate to the two Fe centers in such a way that the Fe−Fe vector serves as a pseudo-C_3 axis and is arranged approximately in a plane parallel to the Cp* planes with the deviation being 0.01 Å. There are no significant differences in the coordination geometry between the two Fe centers. Compared to the Fe−Fe distances of other thiolate-bridged diiron complexes with a Fe−Fe single bond {*cis*-[Fe$_2$(Cp)$_2$(μ-SEt)$_2$(MeCN)$_2$]$^{2+}$ and *cis*-[Fe$_2$(Cp)$_2$(μ-SEt)$_2$(CN)$_2$]} and without a Fe−Fe bond {[PPN][(CN)(CO)$_2$Fe(μ-SEt)$_3$(CO)$_2$(CN)] and [(PR$_3$)(CO)$_2$Fe(μ-SR)$_3$Fe(CO)$_2$(PR$_3$)]$^+$ (R = alkyl)},[11,4a] the short Fe−Fe distance of 2.7723(8) Å in the structure of **1** is clear evidence of an intermetallic bond that falls in the 2.5−2.8 Å range.[12] This bond order observed may closely relate to the spin delocalization over the two Fe centers, which appears in the analogous triply thiolate-bridged ruthenium complex [Cp*Ru(μ_2-SPr)$_3$RuCp*].[7] Complex **2** resembles the core structure of **1** (see Figure S1), except for the two slightly disordered Cp* ligands coordinating to Fe centers.

Reactions of 1 with CO and CN^{t}Bu. In order to understand the reactive properties of **1**, we have further carried out a series of reactions and obtained three new diiron complexes [Cp*FeSEt(μ_2-SEt)$_2$FeCp*CO] (**3**), [Cp*FeSEt(μ_2-SEt)$_2$FeCp*CN^{t}Bu] (**4**), and [Cl$_2$Fe(μ_2-SEt)$_2$FeCp*CN^{t}Bu] (**5**) (Scheme 2). These complexes are all spectroscopically and crystallographically characterized, and the resulting crystallographic data as well as bond distances and angles are presented in Tables 1 and 3.

When it is stirred under CO atmosphere from −78 °C to ambient temperature in THF, a violet solution of **1** changed to a red-brown solution, from which the analytically pure complex **3** is obtained in 74% yield as a red-brown crystalline solid. Unlike the single Cp* signals of **1** and **2**, the ^{1}H NMR spectrum of **3** shows two intense resonances at δ 1.77 and −21.18 ppm assignable to two different Cp* protons, respectively. These two inequivalent Cp* signals are fully consistent with the X-ray structure of **3**. The IR spectrum of **3** (KBr) shows a strong band at 1908 cm^{-1} attributed to C≡O stretching.[7] An ORTEP diagram of **3** is shown in Figure 2. The overall structure consists of two Cp*Fe units bridged by two *syn*-axial SEt ligands, in which the long Fe−Fe distance of 3.4751(11) Å is indicative of the absence of a bonding interaction between the two Fe centers.[11,4a] The SEt and CO ligands occupy the remaining sites of two Fe centers, respectively. The two Cp* ligands are in mutually *cis* orientation with the dihedral angle being 67.7°. The Fe_2S_2 ring is substantially puckered with a dihedral angle of 158.2° along the Fe1−Fe2 vector.

In the same way, treatment of **1** with excess CN^{t}Bu (5 equiv to **1**) in THF from −78 °C to ambient temperature produces **4** in 52% yield as a brown microcrystalline solid, while reaction of **1** under identical conditions in CH_2Cl_2 gives the completely unexpected complex **5** in 73% yield as a dark green solid. The ^{1}H NMR spectrum of **4** shows two intense resonances at δ 2.12 ppm and −18.03 ppm ascribed to two inequivalent Cp* protons, respectively. The ORTEP drawings of **4** and **5** are shown in Figures 3 and 4. The structure of **4** resembles that of **3**. The two Cp* ligands are also in mutually *cis* orientation with dihedral angle being 68.3°. There is no interaction between two iron centers because of the longer Fe−Fe distance of 3.5140(7) Å.[11,4a] The Fe_2S_2 ring is substantially puckered, with a dihedral angle of 158.4° along the Fe1−Fe2 vector. However, the structure of **5** is different from that of **4** in that the two Fe centers are significantly dissimilar in their geometries. The Fe1 center is coordinated by one Cp*, one CN^{t}Bu, and two bridging SEt ligands, while the Fe2 center bonds to two bridging SEt and two Cl ligands, exhibiting a distorted [FeS_2Cl_2] tetrahedral coordination geometry. The nonplanar Fe_2S_2 core has a dihedral angle of 159.1° along the Fe1−Fe2 single bond [2.8939(7) Å].[11,4a] The $\nu_{N\equiv C}$ band at 2047 cm^{-1} is indicative of the terminal end-on coordination mode of the CN^{t}Bu ligand.

The Chemistry Dealing with Carbon−Halogen Bond Cleavage by 4. The formation of **5** is rather unexpected, and this unprecedented example of an organoiron complex in the cleavage of an organic carbon−halogen bond has thus encouraged us to further investigate the potential of this class of clusters as carbon−halogen bond activation reagents (catalysts). Because no reaction occurs between **1** and CH_2Cl_2, **4** may be an important intermediate cleaving the carbon−halogen bond of CH_2Cl_2 in the formation of **5**. Therefore, here we mainly discuss some reactions based on **4** about carbon−halogen bond cleavage.

(11) (a) Vergamini, P. J.; Kubas, G. J. *Prog. Inorg. Chem.* **1976**, *21*, 261–282. (b) Paul, M. T.; Richard, A. C.; Crane, R. M.; Kathleen, R. B.; Douglas, P. *J. Organomet. Chem.* **1991**, *402*, 233–248. (c) Liaw, W. F.; Tsai, W. T.; Gau, H. B.; Lee, C. M.; Chou, S. Y.; Chen, W. Y.; Lee, G. H. *Inorg. Chem.* **2003**, *42*, 2783–2788.

(12) Frisch, P. D.; Lioyd, M. K.; Mccleverty, J. A.; Seddon, D. *J. Chem. Soc., Dalton Trans.* **1973**, 2268–2272.

Table 1. Crystal Data and Structure Refinement for Complexes 1, 2, 3, 4, and 5

	1	2	3	4	5
formula	$C_{26}H_{45}Fe_2S_3$	$C_{38}H_{45}Fe_2S_3$	$C_{27}H_{45}Fe_2OS_3$	$C_{31}H_{54}Fe_2NS_3$	$C_{19}H_{34}Cl_2Fe_2NS_2$
fw	565.50	709.65	593.51	648.63	523.19
temp (K)	293(2)	293(2)	293(2)	293(2)	293(2)
wavelength (Å)	0.71073	0.71073	0.71073	0.71073	0.71073
cryst size (mm)	0.22 × 0.26 × 0.18	0.35 × 0.35 × 0.35	0.36 × 0.20 × 0.04	0.20 × 0.22 × 0.6	0.35 × 0.35 × 0.33
cryst syst	monoclinic	cubic	monoclinic	monoclinic	monoclinic
space group	$P2_1/n$	$I\bar{4}3d$	$C2/c$	$P2_1/n$	$P2_1/n$
a (Å)	10.3794(11)	23.8072(4)	38.895(3)	9.1039(9)	8.9152(3)
b (Å)	17.0781(18)	23.8072(4)	9.2962(6)	33.854(3)	16.2139(4)
c (Å)	15.4868(17)	23.8072(4)	17.9312(11)	11.6173(11)	17.5863(6)
β (deg)	92.412(2)	90.000	115.091(3)	105.452(5)	103.271(2)
V (Å^3)	2742.8(5)	13493.5(4)	5871.7(6)	3451.0(6)	2474.22(13)
Z	4	16	8	4	4
d_{calcd} (g/cm^3)	1.369	1.338	1.343	1.248	1.405
μ (mm^{-1}),	1.298	1.070	1.219	1.042	1.562
$F(000)$	1204	5488	2520	1388	1092
θ (deg)	1.78–26.04	2.10–26.02	2.27–26.37	1.92–23.39	2.51–25.54
limiting indices	$-12 \le h \le 12$	$-19 \le h \le 29$	$-48 \le h \le 48$	$-9 \le h \le 10$	$-10 \le h \le 9$
	$-21 \le k \le 20$	$-29 \le k \le 27$	$-10 \le k \le 11$	$-37 \le k \le 37$	$-19 \le k \le 19$
	$-19 \le l \le 9$	$-29 \le l \le 29$	$-21 \le l \le 22$	$-12 \le l \le 12$	$-21 \le l \le 20$
reflns collected/unique	15 273/5396	36 121/2223	21 238/5755	21 026/4978	9047/4585
GOF(F^2)	0.987	1.080	0.966	1.056	1.003
R_1,[a] wR_2[b] [$I > 2\sigma(I)$]	0.0497/0.0981	0.0465/0.1280	0.0599/0.1383	0.0414/0.1029	0.0468/0.0953
R_1,[a] wR_2[b] (all data)	0.0775/0.1095	0.0550/0.1348	0.1255/0.1736	0.0527/0.1098	0.0842/0.1103
largest diff peak and hole, e Å^{-3}	0.469, −0.339	0.358, −0.271	0.897, −0.376	0.360, −0.288	0.575, −0.255

[a] $R_1 = \sum F_o| - |F_c|/\sum|F_o|$. [b] $wR_2 = \{\sum[w(F_o^2 - F_c^2)^2]/\sum[w(F_o^2)^2]\}2$.

Table 2. Selected Bond Lengths (Å) and Angles (deg) for 1 and 2

1

Bond Distance

Fe(1)−Fe(2)	2.7723(8)	Fe(1)−S(1)	2.2476(11)
Fe(1)−S(2)	2.2736(11)	Fe(1)−S(3)	2.2666(11)
Fe(2)−S(1)	2.2520(11)	Fe(2)−S(2)	2.2804(10)
Fe(2)−S(3)	2.2627(11)		

Bond Angles

S(1)−Fe(1)−S(3)	92.67(4)	S(1)−Fe(1)−S(2)	83.79(4)
S(3)−Fe(1)−S(2)	82.18(4)	S(1)−Fe(1)−Fe(2)	52.04(3)
S(3)−Fe(1)−Fe(2)	52.20(3)	S(2)−Fe(1)−Fe(2)	52.61(3)
S(1)−Fe(2)−S(3)	92.66(4)	S(1)−Fe(2)−S(2)	83.53(4)
S(3)−Fe(2)−S(2)	82.12(4)	S(1)−Fe(2)−Fe(1)	51.89(3)
S(3)−Fe(2)−Fe(1)	52.32(3)	S(2)−Fe(2)−Fe(1)	52.39(3)
Fe(2)−S(3)−Fe(1)	75.48(3)	Fe(1)−S(2)−Fe(2)	75.00(3)
Fe(1)−S(1)−Fe(2)	76.07(4)		

2

Bond Distance

Fe(1)−Fe(2)	2.7351(9)	Fe(1)−S(1)#2	2.2564(13)
Fe(1)−S(1)#1	2.2564(13)	Fe(1)−S(1)	2.2564(13)

Bond Angles

S(1)#2−Fe(1)−S(1)#1	87.65(6)	S(1)#2−Fe(1)−S(1)	87.65(6)
S(1)#1−Fe(1)−S(1)	87.65(6)	Fe(1)−S(1)−Fe(2)	74.32(5)

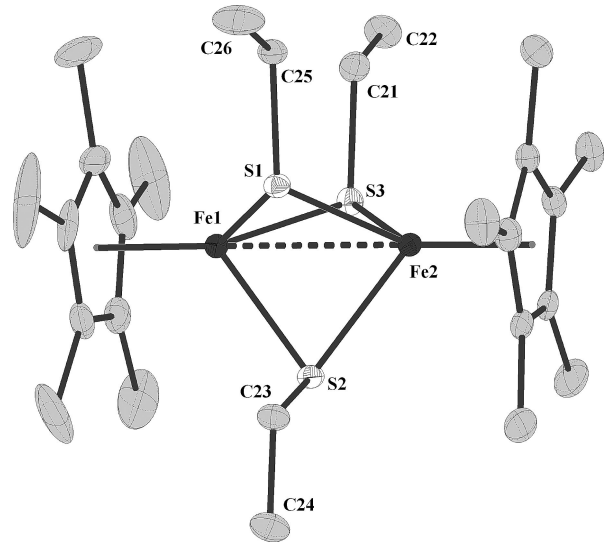

Figure 1. ORTEP (ellipsoids at 30% probability) diagram of **1**. All hydrogen atoms are omitted for clarity.

To obtain some information of cleaving the carbon−halogen bond, we conduct reactions of **4** with chlorohydrocarbon including $CHCl_3$, $CDCl_3$, $PhCH_2Cl$, CH_2Cl_2, CCl_4, and CH_2ClCH_2Cl in THF, as shown in Scheme 3.

When **4** is treated with 5 equiv of $CHCl_3$ in THF at ambient temperature for 12 h, the resulting green solution is evaporated under reduced pressure, and the residue is washed by *n*-hexane to obtain a dark green solid **5** (78% yield). The organic byproducts in the elutropic *n*-hexane solution are analyzed by GC-MS. The mass spectrum of **6** gives a molecular ion $\mathbf{6}^{+\bullet}$ at *m*/*z* 218 (27%), a fragment ion at *m*/*z* 183 (100%) corresponding to the loss of a Cl in the mass spectrum of **6**, and a fragment ion at *m*/*z* 135 (58%) attributed to the loss of $\cdot CHCl_2$ from **6**. The mass spectrum of **7** gives a molecular ion $\mathbf{7}^{+\bullet}$ at *m*/*z* 270 (6%) and a fragment ion at *m*/*z* 135 (100%), which contributes to the loss of $\cdot CH(SEt)_2$. The structures of **6** and **7** are further confirmed by ^{1}H NMR spectrum. In order to confirm such a result, we treat **4** with isotopically labeled $CDCl_3$ instead of $CHCl_3$, giving **5** in 73% yield together with **6**-*d* and **7**-*d*. The mass spectra give a molecular ion $\mathbf{6}$-$d^{+\bullet}$ at *m*/*z* 219 and a molecular ion $\mathbf{7}$-$d^{+\bullet}$ at *m*/*z* 271, respectively.

Similarly, treatment of $PhCH_2Cl$ (5 equiv to **4**) with **4** in THF affords **5** in 65% yield together with **8**[14] and **9**. The mass spectrum of **8** is dominated by a molecular ion at *m*/*z* 152 (29%) and a fragment ion at *m*/*z* 91 (100%). The mass spectrum of **9** is specified by a molecular ion at *m*/*z* 226 (90%) and a fragment ion at *m*/*z* 135 (100%). The structure of **9** is confirmed by ^{1}H NMR, also. The reaction of **4** with CH_2Cl_2 in THF for 3 days at ambient temperature gives **5**, **10**, and **11**, while the reaction

(13) (a) Zimmermann, C.; Anson, C. E.; Eckermann, A. L.; Wunder, M.; Fischer, G.; Keilhauer, L.; Herrling, E.; Pliawa, B.; Hampe, O.; Weigend, F.; Dehnen, S. *Inorg. Chem.* **2004**, *43*, 4595–4603. (b) Toan, T.; Teo, B. K.; Ferguson, J. A.; Meyer, T. J.; Dahl, L. F. *J. Am. Chem. Soc.* **1977**, *99*, 408–416.

Scheme 2

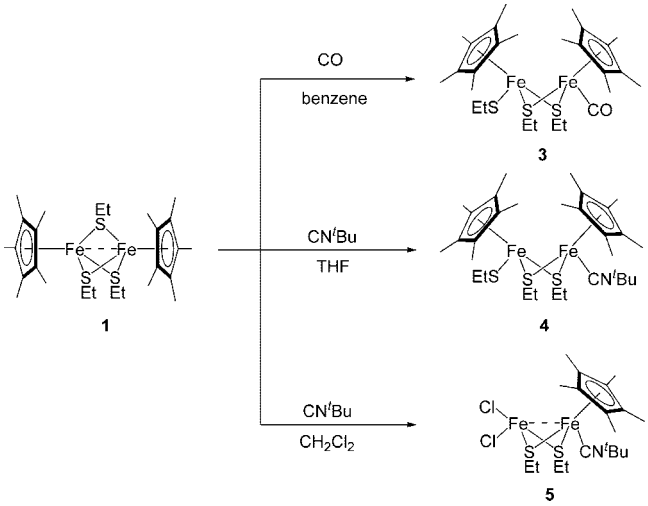

Table 3. Selected Bond Lengths (Å) and Angles (deg) for 3, 4, and 5

		3	
		Bond Distance	
Fe(1)−S(2)	2.2606(15)	Fe(1)−S(3)	2.2664(15)
Fe(2)−S(1)	2.194(2)	Fe(2)−S(2)	2.2914(16)
Fe(2)−S(3)	2.3131(15)	O(1)−C(18)	1.152(6)
Fe(1)−C(18)	1.738(6)		
		Bond Angles	
S(2)−Fe(1)−S(3)	79.93(5)	S(1)−Fe(2)−S(2)	95.00(7)
S(1)−Fe(2)−S(3)	91.89(7)	S(2)−Fe(2)−S(3)	78.32(5)
Fe(1)−S(2)−Fe(2)	99.53(6)	Fe(1)−S(3)−Fe(2)	98.72(5)
		4	
		Bond Distance	
Fe(1)−S(1)	2.2677(10)	Fe(1)−S(2)	2.2552(11)
Fe(2)−S(1)	2.3170(10)	Fe(2)−S(2)	2.3026(10)
Fe(2) −S(3)	2.1987(12)	Fe(1)−C(27)	1.802(4)
N(1)−C(27)	1.155(5)	N(1)−C(28)	1.431(6)
		Bond Angles	
S(2)−Fe(1)−S(1)	78.83(4)	S(3)−Fe(2)−S(2)	95.19(4)
S(3)−Fe(2)−S(1)	94.23(4)	S(2)−Fe(2)−S(1)	76.87(4)
Fe(1)−S(1)−Fe(2)	100.07(4)	Fe(1)−S(2)−Fe(2)	100.88(4)
N(1)−C(27)−Fe(1)	171.5(3)		
		5	
		Bond Distance	
Fe(1)−Fe(2)	2.8939(7)	Fe(1)−S(1)	2.2503(12)
Fe(1)−S(2)	2.2630(11)	Fe(2)−S(1)	2.3423(12)
Fe(2)−S(2)	2.3469(12)	Fe(2)−Cl(1)	2.2416(13)
Fe(2)−Cl(2)	2.2197(14)	Fe(1)−C(15)	1.845(4)
C(15)−N(1)	1.149(5)	N(1)−C(16)	1.465(5)
		Bond Angles	
S(1)−Fe(1)−S(2)	102.54(4)	S(1)−Fe(1)−Fe(2)	52.37(3)
S(2)−Fe(1)−Fe(2)	52.42(3)	Cl(2)−Fe(2)−Cl(1)	114.42(5)
Cl(2)−Fe(2)−S(1)	114.89(5)	Cl(1)−Fe(2)−S(1)	106.27(5)
Cl(2)−Fe(2)−S(2)	110.66(5)	Cl(1)−Fe(2)−S(2)	112.01(5)
S(1)−Fe(2)−S(2)	97.33(4)	Cl(2)−Fe(2)−Fe(1)	114.26(4)
Cl(1)−Fe(2)−Fe(1)	131.28(4)	S(1)−Fe(2)−Fe(1)	49.54(3)
S(2)−Fe(2)−Fe(1)	49.84(3)	Fe(1)−S(2)−Fe(2)	77.74(4)
Fe(1)−S(1)−Fe(2)	78.09(4)		

of **4** with CCl_4 in THF in only 10 min under the same conditions gives **5** and **12**. Compounds **10**, **11**, and **12** are characterized by GC-MS and further characterized by ^{1}H NMR. However, the reaction of **4** with CH_2ClCH_2Cl in THF does not occur at ambient temperature.

Based on the above definitive evidence, it can be seen that **4** can promote the cleavage of carbon−halogen bonds of some chlorohydrocarbons at the Fe center under mild conditions,

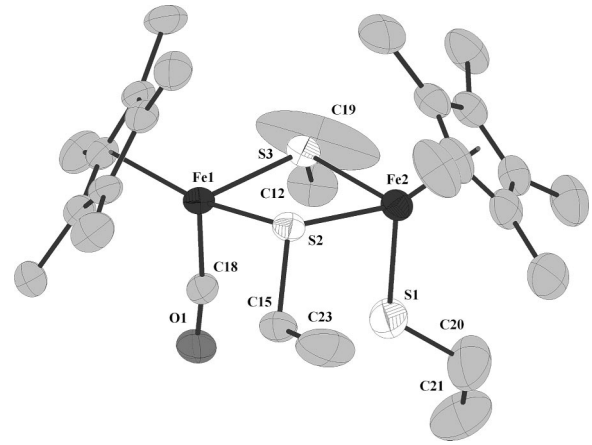

Figure 2. ORTEP (ellipsoids at 30% probability) diagram of **3**. All hydrogen atoms are omitted for clarity.

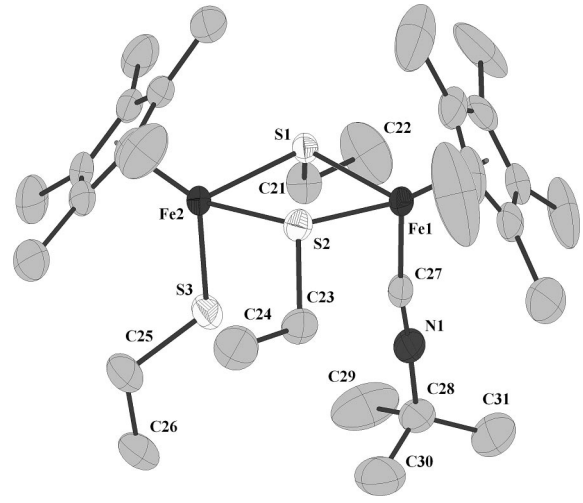

Figure 3. ORTEP (ellipsoids at 30% probability) diagram of **4**. All hydrogen atoms are omitted for clarity.

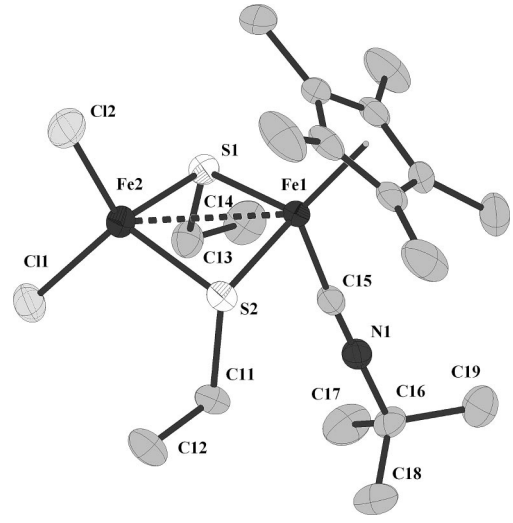

Figure 4. ORTEP (ellipsoids at 30% probability) diagram of **5**. All hydrogen atoms are omitted for clarity.

resulting in the formation of **5** and additional Cp* homologous compounds. The order of reactivity, CCl_4 > $CHCl_3$ > CH_2Cl_2 > CH_2ClCH_2Cl, is consistent with the strength of the carbon−halogen bond. $PhCH_2Cl$ exhibits the greater reactivity,

Scheme 3

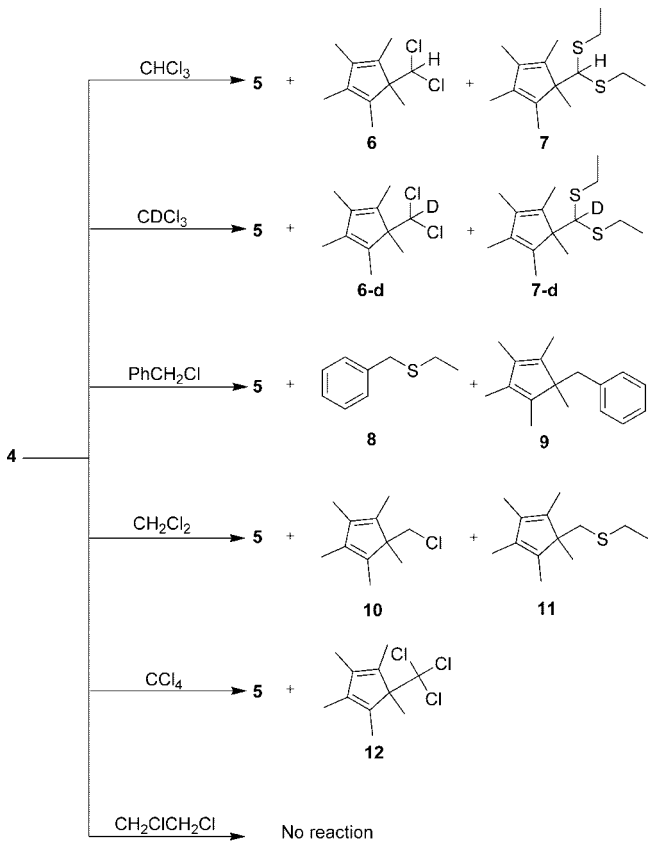

probably owing to the greater stability of the $PhCH_2^+$ intermediate produced by cleaving a carbon−halogen bond.

Electrochemistry. The cyclic voltammogram of **1** has been measured in THF−0.1 M [n-Bu_4N][BF_4], which shows an irreversible oxidation and two quasi-reversible redox peaks. The irreversible oxidation peak at +0.26 V vs Fc/Fc^+ is ascribed to the $[Fe^{II}Fe^{III}] \rightarrow [Fe^{III}Fe^{III}] + e^-$ process. The quasi-reversible redox process observed at $E_{1/2} = -0.90$ V vs Fc/Fc^+ is assigned to $[Fe^{II}Fe^{III}]/[Fe^{II}Fe^{II}]$, and the other at $E_{1/2} = -1.85$ V results from the $[Fe^{II}Fe^{II}]/[Fe^{I}Fe^{II}]$.[7,13]

Experimental Section

General Procedures. All manipulations were routinely carried out under an argon atmosphere, using standard Schlenk-line techniques. All solvents were dried and distilled over an appropriate drying agent under argon. Anhydrous $FeCl_2$ (Aldrich), CN^{t}Bu (Aldrich), HSEt (Aldrich), and HSPh (Aldrich) were used as received. Infrared spectra were recorded on a NEXVS$_{TM}$ FT-IR spectrometer. Element analyses were performed on a Vario EL analyzer. GC-MS spectra were performed on a Hp 6890 GC/5973 MSD analyzer. The ^{1}H NMR spectra were recorded on a Bruker 400 Ultra Shield spectrometer. The EPR spectrum was recorded at room temperature on a Bruker EMX-6/1 EPR spectrometer. Electrochemical measurements were recorded using a BAS-100W electrochemical potentiostat at a scan rate of 200 mV/s. Cyclic voltammograms were obtained in a three-electrode cell under argon in THF−0.1 M [n-Bu_4][BF_4]. The working electrode was a glassy-carbon disk (diameter 3 mm), the reference electrode was a nonaqueous Ag/Ag^+ electrode, and the auxiliary electrode was a platinum wire.

(14) The structure of **8** is established according to standard mass spectral data obtained from Wiley Subscription Services, Inc. (US).

X-ray Crystallography. The data were obtained on a Bruker SMART APEX CCD diffractometer with graphite-monochromated Mo Kα radiation ($\lambda = 0.71073$ Å). Empirical absorption corrections were performed using the SADABS program.[15] Structures were solved by direct methods and refined by full-matrix least-squares based on all data using F^2 using Shelx97.[16] All of the non-hydrogen atoms were refined anisotropically. All of the hydrogen atoms were generated and refined in ideal positions. Two Cp* ligands in **2**, two SEt ligands in **3**, and CN^{t}Bu in **4** were disordered and restrained during refining the structure. Disordered atomic positions were split and refined using one occupancy parameter per disordered group. Crystal data and collection details for **1**, **2**, **3**, **4**, and **5** are given in Table 1.

Preparation of [Cp*Fe(μ_2-SEt)$_3$FeCp*] (1). To a stirred suspension of Cp*Li (6.59 g, 46.38 mmol) in 150 mL of THF was added anhydrous $FeCl_2$ (5.89 g, 46.38 mmol) at 0 °C, followed by stirring for 1 h. The resultant olive-green $[Cp^*FeCl]_2$ solution was cooled to −78 °C. Then, a suspension of LiSEt in THF, which was prepared by reaction of n-BuLi (16.00 mL, 2.9 M solution in n-hexane) and HSEt (3.5 mL, 46.38 mmol) at 0 °C, was transferred via a cannula to the cooled solution of $[Cp^*FeCl]_2$. The mixture was placed in a −78 °C bath for 1 h and stirred overnight as it warmed to room temperature. The resulting red-violet solution was evaporated to dryness, and the residue was purified by column chromatography on neutral alumina with n-hexane as the eluent to give **1** (4.08 g, 49% yield) as a violet microcrystalline solid together with Cp^*_2Fe (1.39 g, 9%). The insoluble solids were washed by water to give Fe(0) (0.38 g, 15%). **1**, ^{1}H NMR (400 MHz, C_6D_6): δ 46.77 (br, 6H), 4.23 (br, 9H), −20.06 (br, 30H). IR (KBr, cm^{-1}): 2958, 2893, 2859, 1477, 1448, 1372, 1226, 1213, 1154, 1065, 1021, 981, 604, 588, 541. Anal. Calcd for $C_{26}H_{45}Fe_2S_3$: C, 55.22; H, 8.02. Found: C, 54.80; H, 8.00.

Preparation of [Cp*Fe(μ_2-SPh)$_3$FeCp*] (2). The reaction was carried out analogously to the procedure described for **1** by using LiSPh (from 0.52 mL of HSPh (4.9 mmol) and n-BuLi (2 mL, 2.5 M solution in n-hexane)). In this case, the resultant dark solid was washed by 5 mL × 3 n-hexane and extracted with benzene. After evaporating the blue solution of **2** in benzene, a microcrystalline solid of **2** was obtained (1.37 g, 55%). ^{1}H NMR (400 MHz, C_6D_6): δ 8.71 (br, 6H), −2.81 (br, 6H), −4.47 (br, 3H), −23.87 (br, 30H). IR (KBr, cm^{-1}): 3049, 2972, 2897, 1575, 1476, 1452, 1435, 1371, 1067, 1019, 1021, 740, 689, 480. Anal. Calcd for $C_{38}H_{45}Fe_2S_3$: C, 64.31; H, 6.39. Found: C, 64.51; H, 6.35.

Preparation of [Cp*FeCO(μ_2-SEt)$_2$SEtFeCp*] (3). When it was stirred under CO atmosphere at −78 °C to room temperature in THF, the violet solution of [Cp*Fe(μ_2-SEt)$_3$FeCp*] (1.11 g, 1.97 mmol) smoothly changed to a red-brown solution. After removal of the volatiles under reduced pressure, the brown residue was washed with 5 mL × 2 acetonitrile to afford the red-brown crystalline solid of **3** (0.86 g, 74%). ^{1}H NMR (400 MHz, C_6D_6): δ 4.50 (br, 6H), 1.65-1.95 (br, 21H), −0.67 (br, 3H), −21.18 (br, 15H). IR (KBr, cm^{-1}): 2950, 2910, 2842, 1908, 1478, 1448, 1374, 1234, 1018, 973, 800, 757, 552. Anal. Calcd for $C_{27}H_{45}Fe_2OS_3$: C, 54.64; H, 7.64. Found: C, 54.90; H, 7.03.

Preparation of [Cp*FeSEt(μ_2-SEt)$_2$FeCN^{t}BuCp*] (4). To a stirred solution of [Cp*Fe(μ_2-SEt)$_3$FeCp*] (0.23 g, 0.41 mmol) in 30 mL of THF was added dropwise CN^{t}Bu (0.26 mL, 2.05 mmol) at −78 °C via a syringe, followed by stirring for 2 h as it warmed to room temperature. The resulting brown solution was evaporated to dryness under reduced pressure. The dark brown residue was washed by a small amount of acetonitrile to obtain a brown crystalline powder, **4** (0.14 g, 52%). ^{1}H NMR (400 MHz, C_6D_6): δ 5.13 (s, 6H), 3.20 (s, 9H), 2.12 (s, 15H), 1.78 (s, 2H), −3.87 (br,

(15) Sheldrich, G. M. *SADABS, Program for Empirical Absorption Correction*; University of Göttingen: Germany, 1996.

(16) Sheldrich, G. M. *SHELX97, Program for Crystal Structure Determination*; University of Göttingen: Germany, 1997.

3H), −18.03 (br, 15H), −21.50 (br, 2H), −26.32 (br, 2H). IR (KBr, cm^{-1}): 2966, 2912, 2047, 1450, 1370, 1234, 1213, 1070, 1022, 977, 802, 756, 520, 482.Anal. Calcd for $C_{31}H_{54}Fe_2NS_3$: C, 57.40; H, 8.39; N, 2.16. Found: C, 57.61; H, 8.35; N, 2.20.

Preparation of [$Cl_2Fe(\mu_2$-SEt)$_2$FeCN^{t}BuCp*] (5). To a stirred solution of [Cp*Fe(μ_2-SEt)$_3$FeCp*] (0.37 g, 0.66 mmol) in 30 mL of CH_2Cl_2 was added dropwise CN^{t}Bu (0.37 mL, 3.30 mmol) at −78 °C via a syringe, followed by stirring overnight as it warmed to room temperature. The resulting green solution was evaporated to dryness under reduced pressure. Then the dark green residue was washed with 10 mL × 3 mixed solvent (*n*-hexane−THF = 1:2) to give a green solid, **5** (0.25 g, 73%). ^{1}H NMR (400 MHz, C_6D_6, 65 °C): δ 2.06 (s, 9H), −2.88-1.09 (m, 10H), −24.06 (br, 15H). IR (KBr, cm^{-1}): 2976, 2905, 2151, 2106, 2083, 2039, 1456, 1377, 1230, 1191, 1020, 1031, 771, 572, 518, 476, 454. Anal. Calcd for $C_{19}H_{34}Cl_2Fe_2NS_2$: C, 43.62; H, 6.55; N, 2.68. Found: C, 43.83; H, 6.33; N, 2.71.

Reaction of 4 with $CHCl_3$. To a brown solution of **4** (0.22 g, 0.36 mmol) in 3 mL of THF was added dropwise $CHCl_3$ (0.20 g, 1.67 mmol) at ambient temperature via a syringe, followed by stirring for 12 h. The resulting green solution was evaporated to dryness under reduced pressure, and the residue was washed by *n*-hexane to obtain a dark green solid, **5** (0.14 g, 78% yield). The organic byproducts **6** (61% yield, GC) and **7** (12% yield, GC) in the elutropic *n*-hexane solution were analyzed by GC-MS and characterized by ^{1}H NMR after being purified by column chromatography. **6**, ^{1}H NMR (400 MHz, $CDCl_3$): δ 5.74 (s, 1H, C*H*Cl_2), 1.83 (s, 6H, Cp*-C*H*$_3$), 1.78 (s, 6H, Cp*-C*H*$_3$), 1.16 (s, 3H, Cp*-C*H*$_3$). MS: *m*/*z* (%) 218 (27), 183 (100), 153 (9), 135 (58), 119 (26), 91 (23), 61 (5), 41 (4). **7**, ^{1}H NMR (400 MHz, $CDCl_3$): δ 3.74 (s, 1H, C*H*), 2.57-2.73 (m, 4H, C*H*$_2$CH$_3$), 1.79 (s, 6H, Cp*-C*H*$_3$), 1.76 (s, 6H, Cp*-C*H*$_3$), 1.25 (t, J = 7.6 Hz, 6H, CH$_2$C*H*$_3$), 1.18 (s, 3H, Cp*-C*H*$_3$). MS: *m*/*z* (%) 270 (6), 147 (6), 135 (100), 119 (6), 107(8), 91 (5), 77 (2).

Reaction of 4 with $CDCl_3$. Treatment of **4** (0.17 g, 0.26 mmol) with $CDCl_3$ (0.16 g, 1.3 mmol) analogously to that described above gave **5** (0.10 g, 73% yield), **6-d** (65% yield, GC), and **7-d** (11% yield, GC). **6-d**, MS: *m*/*z* (%) 219 (25), 184 (100), 169 (8), 149 (8), 135 (60), 119 (25), 105 (14), 91 (16), 63 (4), 41 (4). **7-d**, MS: *m*/*z* (%) 271 (5), 148 (7), 136 (100), 107(8), 91 (5), 64 (1).

Reaction of 4 with $PhCH_2Cl$. Treatment of **4** (0.19 g, 0.30 mmol) with $PhCH_2Cl$ (0.19 g, 1.5 mmol) analogously to that described above gave **5** (0.10 g, 65% yield), **8** (82% yield, GC), and **9** (25% yield, GC). **8**, MS: *m*/*z* (%) 152 (30), 126 (4), 91 (100), 78 (4), 65 (11), 119 (25), 45 (4), 32 (3). **9**, ^{1}H NMR (400 MHz, $CDCl_3$): δ 7.04−7.06 (m, 3H, Ph), 6.83−6.85 (m, 2H, Ph), 2.69 (s, 2H, C*H*$_2$), 1.77 (s, 6H, Cp*-C*H*$_3$), 1.58 (s, 6H, Cp*-C*H*$_3$), 1.00 (s, 3H, Cp*-C*H*$_3$). MS: *m*/*z* (%) 226 (94), 211 (33), 196 (3), 165(5), 135 (100), 119 (42), 104 (26), 91 (37), 65 (7), 41 (4).

Reaction of 4 with CH_2Cl_2. A brown solution of **4** (0.29 g, 0.44 mmol) and CH_2Cl_2 (0.19 g, 2.21mmol) in 3.5 mL of THF was stirred at ambient temperature for 3 days. The resulting green solution was evaporated to dryness under reduced pressure, and the residue was washed by *n*-hexane to give a dark green solid, **5** (0.15 g, 66% yield). The organic byproducts **10** (33% yield, GC) and **11** (10% yield, GC) in the elutropic *n*-hexane solution were analyzed by GC-MS and characterized by ^{1}H NMR after being purified by column chromatography. **10**, ^{1}H NMR (400 MHz, $CDCl_3$): δ 3.43 (s, 2H, C*H*$_2$Cl), 1.78 (s, 6H, Cp*-C*H*$_3$), 1.74 (s, 6H, Cp*-C*H*$_3$), 0.97 (s, 3H, Cp*-C*H*$_3$). MS: *m*/*z* (%) 184 (17), 169 (1), 149 (100), 134 (20), 119 (20), 107 (16), 91 (12), 77 (6), 65 (2), 53 (2), 41 (2). **11**, ^{1}H NMR (400 MHz, $CDCl_3$): δ 2.63 (m, 2H, Cp*-C*H*$_2$S), 2.40 (q, J = 7.6 Hz, 2H, C*H*$_2$CH$_3$), 1.78 (s, 6H, Cp*-C*H*$_3$), 1.72 (s, 6H, Cp*-C*H*$_3$), 1.19 (t, J = 7.6 Hz, 3H, CH$_2$C*H*$_3$), 0.96 (s, 3H, Cp*-C*H*$_3$). MS: *m*/*z* (%) 210 (81), 181 (5), 163 (2), 149 (93), 133(100), 119 (69), 105 (31), 91 (26), 75 (43), 61 (5), 47, (10), 32 (7).

Reaction of 4 with CCl_4. A brown solution of **4** (0.14 g, 0.22 mmol) and CCl_4 (0.17 g, 1.10 mmol) in 3 mL of THF was stirred for only 10 min at ambient temperature. The resulting green solution was evaporated to dryness under reduced pressure, and the residue was washed by *n*-hexane to obtain a dark green solid, **5** (0.10 g, 88% yield). The organic byproduct **12** (83% yield, GC) in the elutropic *n*-hexane solution was analyzed by GC-MS and characterized by ^{1}H NMR after being purified by column chromatography. **12**, ^{1}H NMR (400 MHz, $CDCl_3$): δ 1.95 (s, 6H, Cp*-C*H*$_3$), 1.80 (s, 6H, Cp*-C*H*$_3$), 1.44 (s, 3H, Cp*-C*H*$_3$). MS: *m*/*z* (%) 252 (20), 217 (23), 182 (13), 155 (10), 135 (100), 120 (25), 107 (20), 91 (17), 77 (8), 57 (3), 39, (5).

Conclusion

In summary, two novel thiolate-bridged diiron complexes [Cp*Fe(μ_2-SR)$_3$FeCp*] (R = Et, **1**; R = Ph, **2**) have been successfully prepared through the reactions between the volatile [Cp*FeCl]$_2$ and LiSEt or LiSPh in THF. Complex **1** reacts with CO or CN^{t}Bu to give three new complexes, [Cp*FeSEt(μ_2-SEt)$_2$FeCp*CO], **3**, [Cp*FeSEt(μ_2-SEt)$_2$FeCp*CN^{t}Bu], **4**, and [Cl_2Fe(μ_2-SEt)$_2$FeCp*CN^{t}Bu], **5**. All of these diiron thiolate clusters with single Cp* ligands have been synthesized for the first time. Moreover, the electrochemical behavior of **1** has been discussed simply, and some of the chemistry dealing with carbon−halogen bond cleavage is presented. As the counterparts of diruthenium thiolate clusters, such diiron thiolate clusters with a single Cp* ligand on each Fe center may provide bimetallic reaction sites and simulate biological metalloproteins to activate small molecules. The study of these potential properties including unique catalysis and biological activities is in progress.

Acknowledgment. The authors thank the National Natural Science Foundation of China (No. 20572011) and the Fund for Foreign Scholars in University Research and Teaching Programs of China for financial support of this work.

Note Added after ASAP Publication. The version of this paper published on January 25, 2008, contained the wrong author names in reference 5a. The version that appears now has the correct information.

Supporting Information Available: X-ray crystallographic file (CIF) for complexes **1**, **2**, **3**, **4**, and **5**, and additional figures. This material is available free of charge via the Internet at http://pubs.acs.org.

OM0611148